DESIGN AND CONTROL OF TELE OPERATED MOBILE PLATFORM

AMAREN PRASANNA DAS

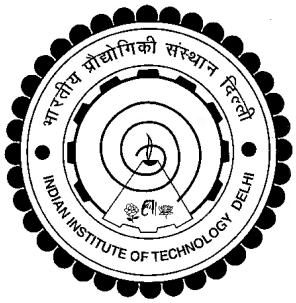

DEPARTMENT OF MECHANICAL ENGINEERING
INDIAN INSTITUTE OF TECHNOLOGY DELHI
OCTOBER 2018

DESIGN AND CONTROL OF TELE OPERATED MOBILE PLATFORM

by

AMAREN P DAS

Department of Mechanical Engineering

Submitted

in fulfillment of the requirements of the degree of Doctor of Philosophy

to the

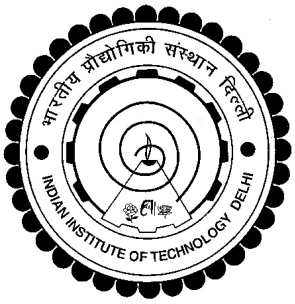

INDIAN INSTITUTE OF TECHNOLOGY DELHI

OCTOBER 2018

Certificate

This is to certify that the thesis entitled **DESIGN AND CONTROL OF TELE OPERATED MOBILE PLATFORM**, submitted by **Shri. Amaren Prasanna Das** to the Indian Institute of Technology Delhi, for the award of the degree of **Doctor of Philosophy** in Mechanical Engineering, is a record of the original, bona-fide research work carried out by him under my supervision and guidance. The thesis has reached the standards fulfilling the requirements of the regulations related to the award of the degree.

The results contained in this thesis have not been submitted in part or in full to any other university or institute for the award of any degree or diploma.

Dr. S. K. Saha

Professor

Department of Mechanical Engineering

Indian Institute of Technology Delhi

New Delhi - 110016, India

Acknowledgements

Amaren P Das

Abstract

XXXXXXXX xx xxxxxxxxxxx XXXX

Contents

List of Figures

List of Tables

Important Symbols and Abbreviations

The important conventions, symbols and abbreviations used in this thesis are listed in the alphabetical order.

Conventions	**Description**
italic	Scalar quantities in lower-case lightface italic with Latin/Greek letters
bold	Vectors are in lower-case boldface Latin/Greek letters
CAPITAL BOLD	Matrices are in upper-case boldface Latin/Greek letters

Latin letters	**Description**
$\mathbf{A}_t$	State transition matrix at time t
a_i, α_i b_i, θ_i	Represents four DH parameters namely, Link length, twist angle, joint offset and joint angle, respectively.
$\mathbf{B}_t$	Control input matrix at time t
$\mathbf{C}$, $\mathbf{C}_i$	Matrix of Convective Inertia (MCI) terms associated with the complete system and the i^{th} subsystem, respectively
f_v	Viscous friction coefficient at the joint of robotic manipulator
f_c	Coulomb friction coefficient at the joint of robotic manipulator
$\mathbf{x}$, $\hat{\mathbf{x}}_{t\|t-1}$	State vector and its estimate at time t with data upto time $(t-1)$
$\mathbf{0}$	Column vector of zeros or null vector with compatible size to the dimensions of the matrices and vectors where it appears
$\mathbf{1}$	Identity matrix of size compatible to the dimensions of the matrices where it appears

Greek letters	Description
α_i	Twist angle of k^{th} link (DH parameter)
θ_i, $\dot{\theta}_i$, $\ddot{\theta}_i$	Relative joint displacement of the i^{th} link, its rate, and acceleration, respectively, in a closed-loop system
$\boldsymbol{\theta_i}$, $\dot{\boldsymbol{\theta}}_i$, $\ddot{\boldsymbol{\theta}}_i$	Vector of relative joint displacement of the i^{th} link, its rate, and acceleration, respectively, in a closed-loop system
$\boldsymbol{\chi}_b$	Vector of base parameters in dynamic model
$\boldsymbol{\lambda}$	Lagrange multiplier representing constraint forces
$\boldsymbol{\omega}_i$	The 3-dimensional angular velocity vector of i^{th} link

Acronyms	
AMM	Aruco Marker Map
ANOVA	Analysis of Variance
VTM	Velocity Transformation Matrix

Functions/Operators	
$\kappa(\mathbf{M})$	Condition number of matrix $\mathbf{M}$
$det(\mathbf{M})$	Determinant of matrix $\mathbf{M}$
$diag(\mathbf{v})$	Element of vector $\mathbf{v}$ at diagonal position of a matrix

Chapter 1

Introduction

The use of robots such as robotic arm has been used in factories for a long time, basically for repetitive kind of job. Though it started with the intention to reduce human labour, production cost and increased productivity. With development of technology , their scope has expanded beyond manufacturing domain. Robots are now being used for health care, surveillance, exploration etc. The reduction in development cost of robotic system has resulted in introduction of robotic system in entertainment industries and personal care. Robots have matured form heavy duty serial linked mechanical arms to a more presentable form such as ASIMO by Haonda and Aibo by Sony.

In areas where human access is not preferred or restricted due to risk of life or inhospitable environmental conditions such as which exists in chemical, space or nuclear industries, robotic systems have gained huge popularity in providing services as surveillance, rescue, exploration & remote maintenance. Research in teleoperated and autonomous mobile robotics has been fuelled largely by these requirement. Teleoperated mobile robots are suitable for these applications as the work space required to be covered is very large and it is essential to maintain physical separation between the robot and its control station, moreover the remote environment is in general unknown.

This research too was motivated by a similar requirement for in-situ mea-

surement of the radioactive radiation, mostly neutron field, inside the vault and cave areas of K-130, K-500 and Medical Cyclotron operational at VECC, Kolkata, West Bengal. Cyclotrons are used to accelerate charged particle beam to high energy. These are required for experiments in nuclear physics and nuclear medicine. The particles are accelerated to high energy using a high frequency alternating voltage which is applied between two hollow "D"-shaped sheet metal electrodes called "Dees" inside a vacuum chamber. The area surrounding the Dee is called the vault and cave is the areas where beam line (beam of accelerated particles) is available for experimentation. Radiation mapping of these areas are mandatory requirements for getting safety clearance from regulators during commissioning of new units and at regular intervals during operational life of the cyclotron facility. Though there are radiation detectors placed at different locations in these area they can only measure radiation levels at discrete location but can not provide the 3-D radiation map. The advantage of having a radiation map is that it provide detailed input to health physicist of the dose a person may receive and accordingly plan emergency operations. These maps also provide the plant operators with the location of radiation leakage and accordingly tune there system to improve its efficiency.

The challenge faced for in-situ inspection during operation of cyclotron is that the interaction between an accelerated beam of charged particles and the target produce Bremsstraghlung and characteristic x-rays, prompt γ-rays, neutrons and delayed radiation (β and γ) thus making human presence unacceptable. A tele-operated mobile robot with wireless communication link is the obvious solution. This thesis discusses design analysis and develop of a prototype robot to carry out in-situ measurement and mapping of radiation level.

1.1 Research Contributions

The original contributions of the present research are listed below:

(i) Design of customized teleoperated mobile robot for remote surveillance and mapping application.

(ii) Development of kinematic and dynamic model of the robot at hand.

(iii) Control architecture required for intuitive tele-operation of this mobile robot.

(iv) Predictive visual feedback control to alleviate problem arising due to time delayed.

1.2 Thesis Organization

The thesis contains eight chapters and one appendix. They are organized as follows:

Chapter 1: Introduction

The present chapter, discusses the scope of mobile robotics in general and the motivation which lead to this research followed by the organization of the thesis.

Chapter 2: Literature Review

This chapter presents the literature review in the following areas *kinamatics and dynamics* of mobile robot, *control of mobile robot*, *control for time delay systems*, *performance of operator under teleopreration* and *predictive display systems.*

Chapter 3: Design of Mobile Platform

This chapter highlights the design considerations of tele-operated mobile platform based on environmental conditions mission requirements. This paper presents the design and control scheme of a mobile manipulator used for radiation survey of Cyclotron vault and cave regions. It discusses the mechanical design for the traction system, the steering gear and the scissor mechanism. Selection of steering system based on terrain condition and power requirement is also discussed.

Chapter 4: Mathematica Modelling of Wheeled Mobile Platform

In this chapter, we present the orthogonal compliment method for deriving the dynamic equation of four wheeled differentially driven platform. The platform has two actuated wheels and two passive wheels. Different types of passive wheels has been studied and there corresponding dynamic equation are presented. The main contribution of this paper is derivation of dynamic equation a differentially driven mobile platform with the most general form of passive wheel.

Chapter 5: Control Architecture

The control architecture and the hardware used for tele-operation is presented along with the detailed description of implementation of the controller software at both the remote (mobile robot) and the local station. The experimental results of robots position based on wheel odometry and is torque requirement for few predefined paths is presented. A comparison study with the simulated results based on dynamic analysis presented in chapter 4 is also presented.

Chapter 6: Simulation Time Delay Tele-operation

In this chapter simulation of a teleoperated mobile platform is presented both under time delay due to communication link and without time delay. It is shown via simulation that with increase in time delay the stability of the teleoperation loop become unstable. A mathematical model of human driver is also presented to simulate the human factor in the teleoperation loop.

Chapter 7: Predictive Display

In this chapter we propose a Predictive Display strategy to counter the time delay in video feedback by extrapolating in time the camera view based on the predicted position of the robot at remote location.

Chapter 8: Conclusions

This chapter summarizes major results of this research work. Limitations along with the future scope from the present experiences are also addressed.

Chapter 2

Literature Review

This chapter presents the survey of the literature highlighting design of different mobile robots and there control either used for field operation or for academic research test platforms.

2.1 Research Objectives

Based on the surveyed literature the objective of the present research are listed below:

- Identify
- To
- To
- Deve
- Es
- To

2.2 Summary

This chapter provided the

Chapter 3

Design of Mobile Platform

Most of the mobile robots presented in literature uses differential wheel drive with passive castor, as in, [1]„ [2] and [3]. The other common methods for locomotion of mobile robots are the omnidirectional wheels [4] and [5], and tracked wheel system [6] and[7] . According to Nagatani [8], a vehicle with Mecanum wheels is susceptible to slippage and same is the case for tracked vehicle, which are inherently skid steered. The slippage of the wheels prevents the most popular dead-reckoning method, using rotary shaft encoders, from being performed well. This chapter discusses the design methodology of a mobile manipulators based on environmental requirements. We also highlights the advantage of Davis steering over castor wheels or other steering methods from the perspective of this mobile manipulator. The Davis steering system modifies the heading of front wheels in a way that, at low speeds, all the wheels are in pure rolling without lateral sliding [9].

3.1 Design Overview

The objective of mobile robot is to navigate inside the cyclotron vault and collect radiation intensity data at all the required points decided by the operator. Data is to be collected not only at different planer locations of the floor but also at varying height from the floor. To cater to this operational requirement, a mobile

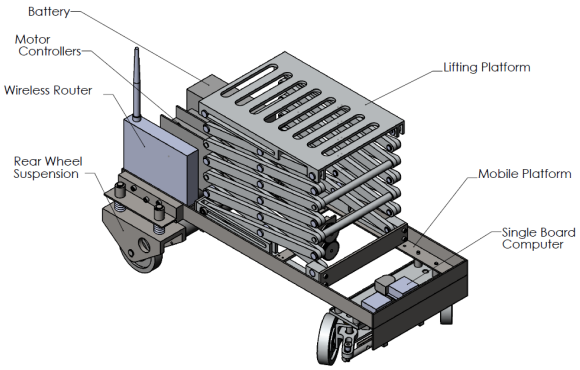

Figure 3.1: 3-D Model of the mobile manipulator

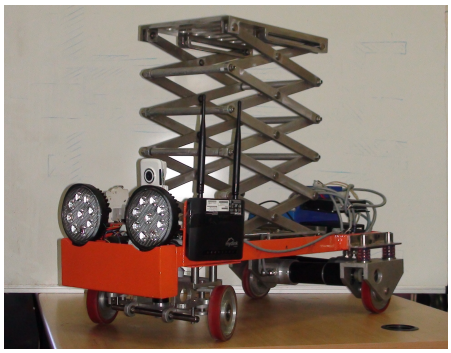

Figure 3.2: Photograph of the actual System

platform with a vertically extendable manipulator arm was developed. Together, they are referred henceforth as mobile-manipulator. The 3-D model of the mobile-manipulator with its major subsystems are shown in Figure 3.1, whereas and the actual system is shown in Figure 3.2.

The environmental condition required that the vehicle be either autonomous or teleoperated. To keep the complexity low it was decided to have wireless teleoperated navigation and control. This gives an operator full flexibility to drive and control the system from a remote station using visual feedback provided by the on board camera. The key parameters of the mobile manipulator are listed in Table 3.1.

Table 3.1: Key parameters and specifications of the mobile manipulator.

Weight	70 Kg	without payload
Payload	10 Kg	—
Footprint	700 mm × 400 mm	-
Height Collapsed	500 mm	Along with Z-Axis
Height Extended	1500 mm	Along with Z-Axis
Steering mechanism	Davis Steering	–
Turning radius	415 mm	-
Ground clarence	45 mm	–
Maximum traction speed	2 m/min	On flat terrain
Ramp climb angle	30°	Checkerboard surface

The mobile-manipulator has a footprint of 700 mm x 400 mm based on the narrow passage which the system has to negotiate. These passages are formed inside the vault area by the pipelines and structural supports of the cyclotron and

its associated equipment. Two DC motors,with speed servo controller, provide the traction to each rear wheels. The two front wheels are inter-connected with Davis steering mechanism [10]. A scissor mechanism provides the vertical motion of the detector.

In order to keep the self weight of the system small all the structural parts are made of aluminum alloy AL6061, apart from the base frame. Stainless Steel (SS304) angle sections is used for the base frame, which give it an excellent strength to weight ratio.

3.1.1 Design of the Traction System

Traction is provided by the two rear wheels driven independently. This makes the system over actuated. A mechanical differential connecting the two rear wheels, as used in cars, would over come this. It was not proposed to do so because; this being a teleoperated vehicle operated in environment inaccessible to human, in case one of the wheel loosing contact with ground due to over hand in small pits or while over an obstacle, the simple differential system will keep supplying power to the free hanging wheel. The system will hence get stuck, maybe in an unrecoverable location. Secondly, in case of one of the actuators failing either the traction or the steering motor, still the system can be manoeuvred to a safe location, albeit with dragging of the wheel with stuck actuator.

Each wheel is driven by a Maxon DC RE50 200W Motor through a 26:1 reduction gearbox. The motors are mounted at an offset to the wheel axis for increased ground clearance. See Figure 3.3. Spring suspension is provided at each wheel to ensure sufficient contact force on uneven ground. The diameter of the wheel is 100 mm (D_w), which is sufficient to ride over obstacle of height 20 mm (Max). They are made of Aluminum alloy-6061 with 5mm thick molded polyurethane (PU) liner. The PU liner provides large traction on cement flooring while being resistance to wear.

The load distribution was optimized to generate maximum normal reaction,

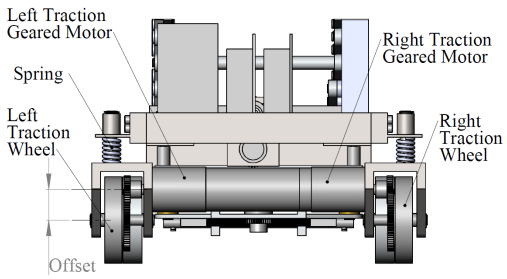

Figure 3.3: Rear Suspension

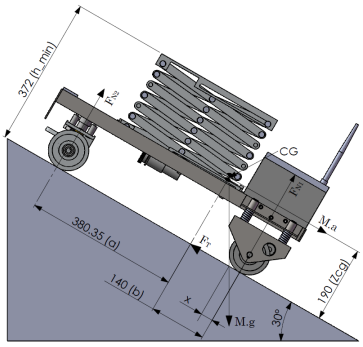

Figure 3.4: Mobile Manipulator on slope

F_n, at the rear wheels without overturning while moving up the ramp of 30^o. Maximizing rear wheel reaction by increasing "b" as per Equation 3.1 ensures increased traction, $F_T = \mu F_N$ (μ is the coefficient of friction), but at the same time decreases the stability margin indicated by "X" in Figure 3.4.

$$F_{N2} = \frac{b}{a} F_{N1}, \quad F_{N1} + F_{N2} = mg\cos\theta \tag{3.1}$$

The stability margin X was fixed as $30mm$ so as to achieve maximum acceleration of $0.144g$ over the ramp of 30^o without overturning. This was done based on the dynamic stability, Equation 3.2.

$$mgb\cos\theta = (mg\sin\theta + ma)z_{cg}, \quad \Rightarrow g(\frac{b}{z_{cg}}\cos\theta - \sin\theta) = a \tag{3.2}$$

where m: mass of vehicle, g: acceleration due to gravity.

3.1.1.1 Selection of Motor and Gearbox

The torque requirement for each rear wheel was calculated based on the static moment balance with the assumption that each rear wheel shares equal load and the total suspended weight is 80 Kg. From the freebody diagram (Figure 3.4), using moment and force balance we get the following:

$$F_{N1} = \frac{aM\cos\theta}{a + b - \mu Z_{cg}}, \qquad F_T = \mu F_{N1} \tag{3.3}$$

In order to estimate the traction motor size, we take worst case scenario $\theta = 0$ and $\mu = 0.3$.

$$F_{N1} = 66Kg, \qquad F_T = 0.3 * 66 \approx 20Kg$$

Since the traction is provided by the two rear wheels. The torque required per wheel (T_w) is given by

$$T_w = (F_T/2)(D_w/2) = (20/2) * 50 = 500Kg - mm \simeq 5Nm \tag{3.4}$$

The motor torque T_M, required based on the assumption of factor of safety, $FS = 1.5$ is

$$T_M = (FS) * T_w = 1.5 * 5 = 7.5 \simeq 8Nm \tag{3.5}$$

Assuming the maximum speed, $V_{ramp} = 1m/s$, of the mobile manipulator over a ramp, the required power, P_M, of the traction motor is calculated as,

$$\begin{aligned} \omega_w &= V_{ramp}/(D_w/2) \simeq 200rpm \\ P_m &= \omega_w T_m = 20 * 8 = 160W \end{aligned} \tag{3.6}$$

The nearest Maxon motor available as per the catalogue [11] is 200W, RE50-370354 motor. The nominal speed, N_s is 5680rpm. Therefore, the gearing ratio required is, $N_s/\omega_w = 5680/200 \simeq 28.4$. The nearest gear box available is of ratio $26:1$, which was chosen.

3.1.2 Design of Steering System

This mobile manipulator uses Davis steering mechanism, Figure 3.5, on the front wheels. Caster were not used as they tend to align with small obstacles and thus get stuck. On the other hand tracked wheels have excellent rough terrain capabilities, but is power intensive due to skid steering. Whereas Omnidirectional wheels need complex controller for coordination.

Davis mechanism satisfies the steering equation 3.7, which ensures pure rolling

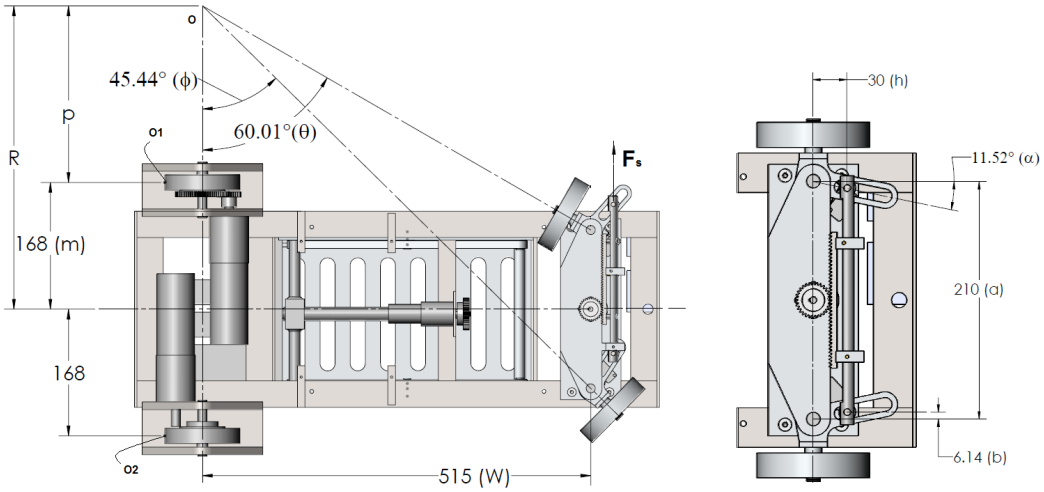

Figure 3.5: Davis steering mechanism

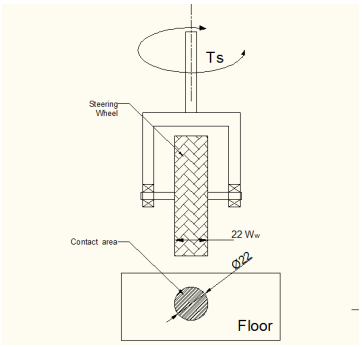

Figure 3.6: Wheel Ground Interaction

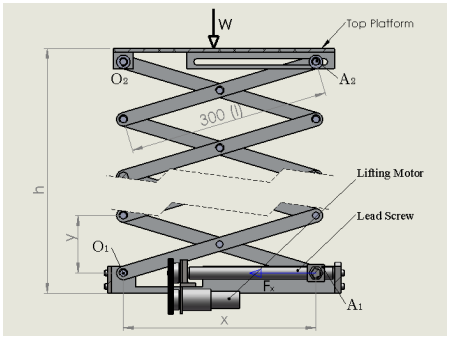

Figure 3.7: Scissor Mechanism

of all wheels over the entire steering range. This makes the system suitable for odometry and energy efficient. The mechanism being positively driven by position controlled servo motor, does not align with the obstacles and thus are able to crossover it. The dimensions of the links used in the steering mechanism is given in Figure 3.5, and are based on the Ackerman steering law given in Equation 3.7

$$\cot\phi - \cot\theta = a/w, \quad \frac{2b}{h} = \frac{a}{w} \tag{3.7}$$

Figure 3.5 shows the extreme values of ϕ and θ, limited by mechanical construction. The minimum turning radius can then be calculated as $a/2 + w\cot\theta = 210/2 + 515\cot 59.8 = 415mm$.

3.1.2.1 Calculation of Steering Torque

The torque required to steer the front wheel is estimated based on a simplified assumption that the wheel deforms under normal load and the contact area thus generated is circular in shape with diameter that of the wheel width, W_w, as shown in Figure 3.6. In order to estimate the normal reaction on each wheel, we assume that the total weight of 80kg is equally shared by the four wheels. Therefore, $N_s = 80/4 = 20Kg$. Next, we apply the uniform pressure formula used to design brakes/clutches, given in Equation 3.8, to find the resistance torque T_s, between the ground and the wheel.

$$T_s = \frac{N_s\mu}{3}W_w = 0.4Nm \tag{3.8}$$

The resistance torque, T_s, of both the wheels are balanced by the force F_s acting on the rack as shown in Figure 3.5. The rack is coupled to the steering motor by a pinion of diameter, $D_p = 40mm$. The motor torque, T_{m_s} in Equation 3.9 is calculated with a high factor of safety, $FS = 3$. This is because T_S is estimated based on a simplified model of brake design. The power, P_{m_s} of the steering motor

based on torque T_{m_s} and the steering speed ω_s of 100rpm is

$$T_{m_s} = (FS)\frac{2T_s}{h}\frac{D_p}{2} = 1.6Nm \quad \text{and} \quad P_{m_s} = T_{m_s} * \omega_s = 17W \tag{3.9}$$

Based on the above specifications, a 20W, RE25 DC motor of Maxon make and a gear box GP32 of ratio 159:1 was chosen for the steering mechanism.

3.1.3 Design of Scissor Mechanism

The vertical stage was designed to move up to a height of 1.5m from the floor level. This motion was generated using a scissor mechanism, as shown in Figure 3.7. The scissor mechanism has two major advantages over other lifting methods such as telescopic pillar, etc. First, the ratio of height in extended and collapsed condition is very large. In our case it is 3 : 1. Second, the self weight of the mechanism is very low as it is made of rectangular links.

The scissor mechanism, figure 3.7, has 6 stages, where one "X" denotes one stage. The Scissor is connected to the top platform by a pivot joint O_2 and a prismatic joint A_2. This is coupled to the base frame by pivot joint O_1 and a prismatic joint A_1. The linear actuation of joint A_1 is provided by a lead screw of pitch (P) 1.5 mm and mean diameter (d_m) 10mm. This results in vertical motion of the top platform. From geometry we get

$$\begin{aligned} &y = l\sin\theta,\ x = l\cos\theta,\ \Rightarrow dy = l\cos\theta d\theta,\ dx = -l\sin\theta d\theta \\ &h = Ny \rightarrow dh = Ndy \end{aligned} \tag{3.10}$$

Where, N=6 is number of stages. From the principle of virtual work, we get

$$-F_x dx = W dh,\ \Rightarrow F_x = \frac{WN}{\tan\theta} \tag{3.11}$$

Where, F_x is the axial force on the prismatic joint, A_1 and W is the payload. From Equation 3.11, it is clear that as $\theta \rightarrow 0$, the force $F_x \rightarrow \infty$. In the present design

$\theta_{min} = 5^o$ and $\theta_{max} = 45^o$. Therefore, the extended height $h_{max} = Nl \sin\theta_{max} = 1.3m$ and the collapsed height $h_{min} = 156mm$. The maximum force $F_x = 342Kg$ is required at $\theta_{min} = 5^o$, assuming $W = 8kg$ as payload. This was used in formula for screw jack [10] , Equation 3.12, to calculate the motor torque of the scissor mechanism.

$$T_L = \frac{F_x d_m}{2}\left(\frac{p + \pi\mu d_m \sec\alpha}{\pi d_m - \mu p \sec\alpha}\right) = 7.5Nm \tag{3.12}$$

Where coefficient of friction, $\mu = 0.1$, ACME thread angle $2\alpha = 60^o$ and pitch $p = 1.5mm$ is used. Based on the above specification 10W RE20 DC motor with a gear box of 25:1 ratio is chosen from Maxon motor catalogue [11].

3.2 Conclusion

Design calculation for a mobile manipulator are presented in this paper. Different aspects based on the requirements of radiation inspection around cyclotron was taken into account. Advantage of positively steered wheels over caster wheel was highlighted for mobile robots.

Chapter 4

Mathematica Modelling of Wheeled Mobile Platform

In the field of mobile robotics extensive research has been carried out. Mobile robots can broadly be divided into three categorises-wheeled robots, legged robots [12] and aerial vehicles [13]. There are few mobile robots which uses both wheels and legs for locomotion for example the Creadapt [14], in order to take advantage of both modes of locomotion. Among these the most extensively studied are the Wheeled mobile robots (WMR). They have been classified in to five generic classes by Champion et.al [15], [16] based on there mobility resulting from the kinematic constrains due to different wheel types. The most common among these are the 3 wheeled differential driven WMR with one castor wheels. Because of its simplicity in modelling, they have been used in most of the control and motion planing algorithm [17], [18] and [19].

In order to develop a model based control algorithm it is imperative to have good dynamic model of the WMR. These dynamic models are used in simulation software, Software in Loop (SIL) testing and Hardware in Loop testing of controllers. Different methods has been adopted to derive the dynamic model of WMR. A general dynamical model is derived for three-wheel mobile robots with nonholonomic constraints by using a Lagrange formulation by B. d'Andrea-Novel

[20]. Where as Thanjavur and Rajagopalan [21] has used Kane's method and Saha et. al. [22],[3] uses natural orthogonal compliment (NOC) method.

All the papers known to us uses, the standard caster wheel in deriving the dynamic model of the WMR. In this paper we have presented the modelling of Castor wheel in the most general configuration. In the stranded castor wheel the axis of rotation is perpendicular to the line joining the pivot and the axis of rotation as shown in Figure 4.2. Where as in our case they oriented in the most general way as shown in figure Figure 4.1. We have used the Natural Orthogonal Compliment approach as it inherently takes care of the non-holonomic constraint of the wheels. Moreover being a matrix based approach it is convenient for numerical simulations. The paper is divide in to three parts in the first part we briefly introduce the concept of NOC method, in the second part the derivation of dynamic model of WMR is presented, in the last part we discuss few special cases which can be derived from our model.

4.1 Natural Orthogonal Compliment (NOC) Method

Let us consider a system n rigid body, interconnected with different types of joints. Let, f_i be the net force acting at the center of mass (CM) of the $i-th$ body and n_i is the net moment. If m_i is the mass, I_{ci} moment of inertia with respect to CM, c_i position vector of CM and ω_i the angular velocity of the same body. Then equation of motion of $i-th$ rigid body is given by Newton-Euler equations 4.1.

$$f_i = m_i\ddot{c}_i \quad and \quad n_i = I_{ci}\omega_i + \omega_i \times I_{ci}\omega_i \tag{4.1}$$

If we define, twist (t) and wrench(w) as

$$t_i = \begin{pmatrix} \omega_i \\ \dot{c}_i \end{pmatrix} \quad w_i = \begin{pmatrix} n_i \\ f_i \end{pmatrix}$$

The wrench w_i acting on the $i-th$ body can be decomposed into w_i^w, called the *working component* and w_i^C, the *non-working component*. The working component consists if all the forces and torques, which imparts/extracts energy to/from the system, i.e. motor actuating torque. The non-working component of the wrench consists of the forces and torques which are used to constrain the motion of the body at the joints. Then Newton-Euler Equation (4.1) can be rewritten in a single matrix equation as

$$M_i\dot{t}_i + W_i M_i t_i = w_i^w + w_i^c \quad \because w_i = w_i^w + w_i^c \tag{4.2}$$

$$M_i = \begin{pmatrix} I_{ci} & 0 \\ 0 & m_i\tilde{1} \end{pmatrix}, \quad W_i = \begin{pmatrix} \Omega_i & 0 \\ 0 & 0 \end{pmatrix}, \quad \Omega_i = \omega_i \times \tilde{1} \tag{4.3}$$

Where $\omega_i \times 1$, is refered as the cross product matrix of vector ω_i and $\tilde{1}$, denotes the identity matrix, for details refer to [23],[24]. The equation of all the n rigid body in the system can be collected and written as a single matrix equation (4.4) referred to as decoupled equation of motion of the system.

$$M\dot{t} + WMt = w^c + w^w \tag{4.4}$$

Where

$$M = diag[M_1, M_2, ...M_n[, \quad W = diag[W_1, W_2, ...W_n], \quad t = [t_1^T, t_2^T, ...t_n^T]^T$$

$$w^j = [{w_1^j}^T, {w_2^j}^T, ...{w_n^j}^T]^T,\ j = c, w$$

The kinematic constraint both holonomic and non-holonomic (i.e. pure rolling) between two bodies i and j of a system, give rise to linear homogeneous system of algebraic equations [23] as given below, where A_i, A_j depend on the DH parameters.

$$A_i t_i + A_j t_j = 0 \tag{4.5}$$

The constraint equations corresponding to all the joints in the system can be written in terms of the *generalized twist vector* t. Furthermore if, $\dot{\theta} = (\dot{\theta_1}, \dot{\theta_2}, ...)$ denote the *independent generalized velocity* of the system, we can then write t in terms of $\dot{\theta}$ as $t = T\dot{\theta}$. Using the fact, that $\dot{\theta}$ can take any arbitrary value, we get

$$At = 0, \quad \Rightarrow AT\dot{\theta} = 0 \quad \Rightarrow AT = 0 \tag{4.6}$$

The above equation (4.6) indicates that T is the orthogonal compliment of A. Since this relation arises naturally, hence the name *Natural Orthogonal Compliment*. It can be shown [23] that the non-working wrench w^c, lies in the range space of A^T. In view of equation 4.6, it can be proved that w^c lies in the null space of T^T, therefore

$$T^T w^c = 0 \tag{4.7}$$

To eliminate the non-working forces and moments, i.e w^C from the uncoupled equation of motion (4.4), we multiply both sides of equation 4.4 by T^T.

$$T^T M\dot{t} + T^T WMt = T^T w^W, \quad \Rightarrow T^T MT\ddot{\theta} + T^T(M\dot{T} + WMT)\dot{\theta} = T^T w^T \tag{4.8}$$

Equation 4.9 represents the dynamic equation of interconnected n-body system. This equation can be expressed in terms of the independent generalized velocity $\dot{\theta}$ and generalized acceleration $\ddot{\theta}$, by using the relations $t = T\dot{\theta}$ and $\dot{t} = \dot{T}\dot{\theta} + T\ddot{\theta}$ in equation 4.9. thus the final equations of motion can be written as

$$or \qquad I(\theta)\ddot{\theta} = C(\theta, \dot{\theta})\dot{\theta} + \tau \tag{4.9}$$

Where

$$I(\theta) \equiv T^T MT, \text{generalized inertia matrix}$$

$$C(\theta, \dot{\theta}) \equiv -T^T(M\dot{T} + WMT)\dot{\theta}, \text{convective inertia matrix}$$

$$\tau \equiv T^T w^T, \text{ generalized driving force vectcor}$$

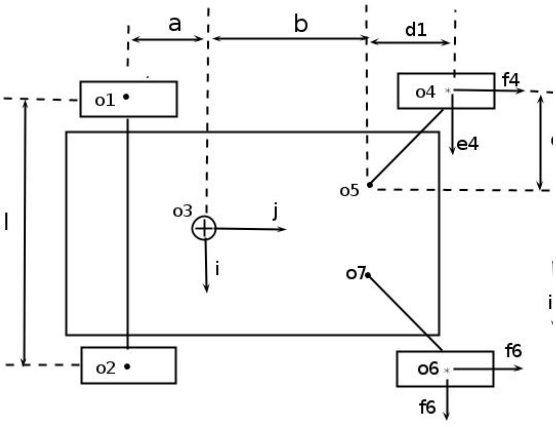

Figure 4.1: WMR-general

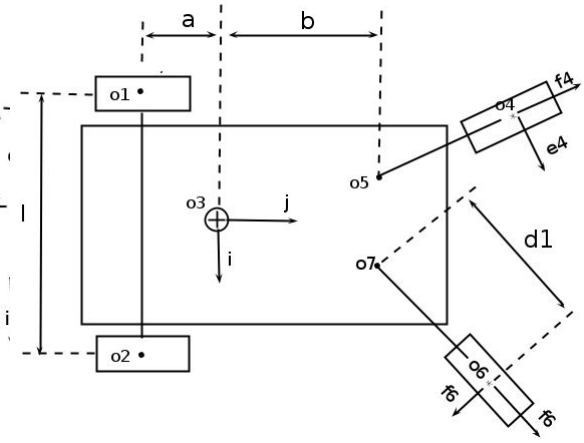

Figure 4.2: WMR-Std. Castor

Figure 4.3: Castor wheel Configuration of WMR

4.2 Dynamic Equation of WMR

The dynamic equation of a differentially driven 3 wheeled mobile platform based on Natural orthogonal compliment metohod has been presented by Saha[22]. The vehicle consisted of 2 driven wheel and one standard caster wheel.In general for large vehicles it necessary to have at least four wheels, for the point of stability of the vehicle.Such a vehicle is shown in figure 1. It may be noted that the caster wheels used in this case are the standered caster wheel configuration, where the angle between line O_4O_3 and vector e_3 is 90 deg. This is a special case of the more general configuration of the caster wheel which are shown in figure 2, where angle between line O_4O_3 and vector e_3 is not 90 deg

The vehicle we have considered in this paper is shown in figure 2. It consist two independently driven wheels at the back and two generalized caster wheels at the front. The actuated wheels are labelled as body #1 and #2. The platform is body #3, The first caster wheel and its bracket is labelled as #4 and #5, with the castor pivoted at O_4. Similarly the second castor is pivoted at O_6, and its bracket and wheel is labelled as #6 an #7. All the wheels are assumed to be rolling with out slipping.

4.2.1 Kinematic analysis

In order to proceed with the kinematic analysis of the vehicle in figure 1, we define a orthogonal triad of vectors i, j, k at point O_3, the control point of the platform, as shown in the figure. If $\dot{\theta_1}$ and $\dot{\theta_2}$ denotes the rate of rotation of wheel #1 and #2. Then the linear velocity of point O_1&O_2 under pure rolling condition is given by

$$\dot{O_i} = r\dot{\theta_j}, \quad \text{r=radius of wheel} \tag{4.10}$$

The angular velocity of the platform ω_3 can be written as

$$\omega_3 = (r/l)(\dot{\theta_1} - \dot{\theta_2}). \tag{4.11}$$

Further, the velocity of point o_3 can be written as $\dot{o_3} = \dot{o_i} + \omega_3 \times (c - o_i), \quad i = 1, 2.$ where, o_3 and o_i is the position vector of point O_3 and O_i respectively, with respect to some point fixed to the ground. By eliminate ω_3 from these two equation, we get

$$\dot{o_3} = (ar/l)(\dot{\theta_1} - \dot{\theta_2}) + (r/2)(\dot{\theta_1} + \dot{\theta_2}) \tag{4.12}$$

Now, the the angular velocity of the drive wheel #1 can be expressed as $\omega_1 = -\dot{\theta_1} i + \omega_3 k$, using equation 4.11, we can write

$$\omega_1 = \begin{pmatrix} -i + (r/l)k & -(r/l)k \end{pmatrix} \begin{pmatrix} \dot{\theta_1} \\ \dot{\theta_2} \end{pmatrix} \tag{4.13}$$

Using equation 4.10 and 4.13, we can write the twist for wheel #1 in terms of $\dot{\theta_a}$, as

$$t_1 = \begin{pmatrix} \omega_1 \\ \dot{o_1} \end{pmatrix} = \begin{pmatrix} -i + (r/l)k & -(r/l)k \\ rj & 0 \end{pmatrix} \begin{pmatrix} \dot{\theta_1} \\ \dot{\theta_2} \end{pmatrix} \tag{4.14}$$

Similarly, for the other actuated wheel #2, we get

$$t_2 = \begin{pmatrix} \omega_1 \\ \dot{o_1} \end{pmatrix} = \begin{pmatrix} -i + (r/l)k & -(r/l)k \\ 0 & rj \end{pmatrix} \begin{pmatrix} \dot{\theta_1} \\ \dot{\theta_2} \end{pmatrix} \tag{4.15}$$

To calculate the twist, t_3 of the platform, body #3, we use combine equation 4.11 and 4.12, and get

$$t_3 = \begin{pmatrix} \omega_3 \\ \dot{o_3} \end{pmatrix} = \begin{pmatrix} \rho\delta & -\rho\delta \\ r(\lambda i + (1/2)j & r(-\lambda i + (1/2)j \end{pmatrix} \begin{pmatrix} \dot{\theta_1} \\ \dot{\theta_2} \end{pmatrix} \tag{4.16}$$

where

$$\delta \equiv d/l, \quad \rho \equiv r/d, \quad \lambda \equiv a/l$$

In order to calculate the twist of the caster bracket and the caster wheel, we need to express the unactuated joint rates $\dot{\psi_1}$ and $\dot{\phi_1}$, in terms of actuated angle rate vector $\dot{\theta_a}$. Where, $\dot{\psi_1}$ denotes the rate of rotation of bracket, body #5 about O_4 with respect to the platform, and $\dot{\phi_1}$ the rate of rotation of caster wheel, body #4 about its axis e_3, with respect to bracket. The velocity of O_5 can be expressed in two independent forms, one in terms of the velocity of o_3 and the other in terms of the velocity of o_5, i.e

$$\dot{o_5} = \dot{o_4} + \omega_5 \times (d_1 e_4 - d2 f_4), \quad \dot{o_5} = \dot{o_4} + \omega_5 \times (d_1 e_4 - d2 f_4) \tag{4.17}$$

On equating the above to equations together, and using the rotation matrix between coordiante system $\{i, j, k\}$ and $\{e_4, f_4, k\}$, to express the equation in $e_4 \& f_4$, we get

$$(-\dot{\phi_1} r + \dot{\psi_1} d_1) f_3 + d_3 \dot{\psi_1} e_3 = \dot{o_3} + \omega_3 (m \cos\psi_1 - b \sin\psi_1 - d_1) e_4 \tag{4.18}$$

Taking the dot product of the above equation first with e_4 and then with f_4, and

using equation 4.12 for $\dot{o_3}$, we get

$$\begin{pmatrix} d_2 & 0 \\ -d_1 & r \end{pmatrix} \begin{pmatrix} \dot{\psi_1} \\ \dot{\phi_1} \end{pmatrix} = \begin{pmatrix} (-ar/l)S_{\psi_1} + (r/2)C_{\psi_1} + \delta_1 & (ar/l)S_{\psi_1} + (r/2)C_{\psi_1} - \delta_1 \\ (ar/l)C_{\psi_1} + (r/2)S_{\psi_1} + \delta_2 & (-ar/l)C_{\psi_1} + (r/2)S_{\psi_1} - \delta_2 \end{pmatrix} \dot{\theta_a} = [F_{ij}]\dot{\theta_a} \tag{4.19}$$

where,

$$\delta_1 = (r/l)(mC_{\psi_1} - bS_{\psi_1} - d2, \quad \delta_2 = (r/l)(mS_{\psi_1} + bC_{\psi_1} + d1$$

Similarly for the other caster wheel we get,

$$\begin{pmatrix} d_2 & 0 \\ -d_1 & r \end{pmatrix} \begin{pmatrix} \dot{\psi_2} \\ \dot{\phi_2} \end{pmatrix} = \begin{pmatrix} (-ar/l)S_{\psi_2} + (r/2)C_{\psi_2} - \delta_3 & (ar/l)S_{\psi_2} + (r/2)C_{\psi_2} + \delta_3 \\ (ar/l)C_{\psi_2} + (r/2)S_{\psi_2} + \delta_4 & (-ar/l)C_{\psi_2} + (r/2)S_{\psi_2} - \delta_4 \end{pmatrix} \dot{\theta_a} = [G_{ij}]\dot{\theta_a} \tag{4.20}$$

where,

$$\delta_3 = (r/l)(mC_{\psi_2} + bS_{\psi_2} + d2, \quad \delta_4 = (r/l)(mS_{\psi_2} + bC_{\psi_2} + d1$$

The angular and the liner velocity of the c.g.of the caster wheel,#4 is written in-terms of the co-ordinate frame fixed to the bracket #5, $\{e_4, f_4, k\}$, as

$$\omega_4 = \dot{\phi_1}e_4 + (\omega_3 + \dot{\psi_1})k, \quad \dot{o_4} = \dot{\phi_1}e_4 \tag{4.21}$$

Using equation 4.19 and 4.11, the twist t_4 can be written as

$$t_4 = \begin{pmatrix} \Theta_4 \\ C_4 \end{pmatrix} \dot{\theta_a} \tag{4.22}$$

where

$$\Theta_4 = [F_{11}e_4 + \bar{F_{21}}k \quad F_{12}e_4 + \bar{F_{22}}k], \quad C_4 = r[-F_{11}f_4 \quad - F_{12}f_4]$$

$$\bar{F_{21}} = F_{21} + \rho\delta, \quad \bar{F_{22}} = F_{22} - \rho\delta$$

The angular and the liner velocity of the c.g.of the caster bracket,#5 is written in-terms of the co-ordinate frame fixed to the bracket, as

$$\omega_4 = \dot{\phi}_1 e_3 + \dot{\psi}_1 k, \quad \dot{o_4} = \dot{o_4} + \omega_5 \times [-df_3] \tag{4.23}$$

Now using equations4.19& 4.11, the twist t_5 can be written as

$$t_5 = \begin{pmatrix} \Theta_5 \\ C_5 \end{pmatrix} \dot{\theta_a} \tag{4.24}$$

where

$$\Theta_5 = [\bar{F_{21}} k \quad \bar{F_{22}} k], \quad C_5 = d[(1/2) bar F_{21} e_4 - \rho F_{11} f_4 \quad (1/2) bar F_{22} e_4 - \rho F_{12} f_4]$$

In similar manner the twist t_6&t_7 of the other caster wheel and its bracket can be written as

$$t_6 = \begin{pmatrix} \Theta_6 \\ C_6 \end{pmatrix} \dot{\theta_a}, \quad t_7 = \begin{pmatrix} \Theta_7 \\ C7 \end{pmatrix} \dot{\theta_a} \tag{4.25}$$

where

$$\Theta_6 = [G_{11} e_6 + \bar{G_{21}} k \quad G_{12} e_6 + \bar{G_{22}} k], \quad C_6 = r[-G_{11} f_6 \quad - G_{12} f_6]$$

$$\Theta_7 = [\bar{G_{21}} k \quad \bar{G_{22}} k], \quad C_7 = d[(1/2) bar G_{21} e_6 - \rho G_{11} f_6 \quad (1/2) bar G_{22} e_6 - \rho G_{12} f_6]$$

$$\bar{G_{21}} = G_{21} + \rho\delta, \quad \bar{G_{22}} = G_{22} - \rho\delta$$

Dynamic Equations

Based on the twist calculated in terms of the independent actuation vector $\dot{\theta_a}$, we now derive the generalized inertia matrix and the Convective inertia term for the coupled equation of motion 4.9.

Generalized Inertia Matrix, I

From the above equations of twist of individual body we get $t_i = T_i\dot{\theta_a}$, by definition $t = [t_1^T, t_2^T....t_7^T]^T$. Therefore, we get

$$T = [T_1^T, T_2^T, ...T_7]^T$$

. Since the matrix M is block diagonal

$$I = T^T M T = T_1^T M_1 T_1 + T_2^T M_2 T_2 + ...T_7^T M_7 T_7 \tag{4.26}$$

$$I_m = \sum_{i=1,2} T_i^T M_i T_i = \begin{pmatrix} I_w + (\rho\delta)^2 H + + m_w r^2 & -2(\rho\delta)^2 H \\ -2(\rho\delta)^2 H & I + (\rho\delta)^2 H + + m_w r^2 \end{pmatrix} \quad \texttt{where} M_i = \begin{pmatrix} I_w & 0 \\ 0 & m_w \mathbf{1} \end{pmatrix} \tag{4.27}$$

Where $\tilde{I_w} = \begin{pmatrix} I_w & 0 & 0 \\ 0 & H & \\ 0 & 0 & H \end{pmatrix}$ is the 3×3 moment of Inertia matrix expressed in co-ordinate $\{i, j, i\}$, m_w is the mass of the motorized wheels, and 1 is3×3 identity matrix.

If the mass of the platform is m_p and its moment of inertia about vector $\mathbf{k}$ is I_p, then [23]

$$I_3 = T_3^T M_3 T_3 = I_p(\rho\delta)^2 \begin{pmatrix} 1 & -1 \\ -1 & 1 \end{pmatrix} + m_p r^2 \begin{pmatrix} (1/4) + \gamma^2 & (1/4) - \gamma^2 \\ (1/4) - \gamma^2 & (1/4) + \gamma^2 \end{pmatrix} \tag{4.28}$$

Similarly,if m_c is the mass of the castor wheel and it is assumed to be a solid disk, then the generalized inertia matrix can be written as

$$I_c = \sum_{i=4,6} T_i^T M_i T_i = (m_c r^2/4) \begin{pmatrix} 6F_{11}^2 + \bar{F_{21}}^2 & 6F_{11}F_{12} + \bar{F_{21}}\bar{F_{22}} \\ 6F_{11}F_{12} + \bar{F_{21}}\bar{F_{22}} & 6F_{12}^2 \bar{F_2} 2 \end{pmatrix} + \begin{pmatrix} 6G_{11}^2 + \bar{G_{21}}^2 & 6G_{11}G_{12} + \\ 6G_{11}G_{12} + \bar{G_{21}}\bar{G_{22}} & 6G_{12}^2 \end{pmatrix} \tag{4.29}$$

If the mass of the brackets i.e. body #5 and #7 are small compared to the mass of the caster wheels, then contribution of $T_5^T M_5 T_5$ and $T_7^T M_7 T_7$ can be assumed

to be zero.

Convective Inertia matrix C

The Convective inertia term of equation 4.9 can be broken down in to two parts, $T^T M\dot{T}$ and $T^T WMT$. Since the generalized inertia matrix of the motorized wheels and the platform is constant, they do not contribute to either of these terms. Moreover we have considered the mass of the brackets to be zero, so they also do not contribute to convective inertia term. Hence

$$C = T^T M\dot{T} + T^T WMT = \sum_{i=4,6} T_i^T M_i \dot{T}_i + \sum_{i=4,6} T_i^T W_i M_i T_i \tag{4.30}$$

The expression for the first term is found by using equations 4.19,4.20,4.22 and 4.25. $\dot{F_{ij}}$ and $\dot{G_{ij}}$ denotes the derivative of the elements of matrix F and G defined in 4.19,4.20 . To find $\dot{T}_4 \& \dot{T}_6$ we have used the fact $\dot{e_4} = \omega_4 \times e_4$ and $\dot{e_4} = \omega_6 \times e_6$.

$$\begin{aligned} T^T M\dot{T} = (m_c r^2/4)\Bigg[& \begin{pmatrix} 6F_{11}\dot{F_{11}} + \bar{F_{21}}\dot{F_{21}} & 6F_{11}\dot{F_{12}} + \bar{F_{21}}\dot{F_{22}} \\ 6\dot{F_{11}}F_{12} + \dot{F_{21}}\bar{F_{22}} & 6F_{12}^2\bar{F_{22}} \end{pmatrix} \\ & + \begin{pmatrix} 6G_{11}\dot{G_{11}} + \bar{G_{21}}\dot{G_{21}} & 6G_{11}\dot{G_{12}} + \bar{G_{21}}\dot{G_{22}} \\ 6\dot{G_{11}}G_{12} + \dot{G_{21}}\bar{G_{22}} & 6G_{12}^2\bar{G_{22}} \end{pmatrix} \Bigg] \end{aligned} \tag{4.31}$$

The second term of equation 4.31 evaluates to zero, as shown below. Consider castor wheel, body #4. Using equation 4.22 and definition of W defined in 4.3 we get,

$$T_4^T W_4 M_4 T_4 = [\Theta_4, C_4] \begin{pmatrix} \Omega_4 & 0 \\ 0 & 0 \end{pmatrix} \begin{pmatrix} I_4 & 0 \\ 0 & m_4 \mathbf{1} \end{pmatrix} \begin{pmatrix} \Theta_4 \\ C_4 \end{pmatrix} = \Theta_4 \Omega_4 I_4 \Theta_4 \tag{4.32}$$

To evaluate the above equation, we express all the terms in the coordinate

system $\{\mathbf{e_4}, \mathbf{f_4}, \mathbf{k}\}$.

$$\Theta_4 = \begin{pmatrix} F_{11} & 0 & F_{12} \\ 0 & 0 & 0 \\ \bar{F_{21}} & 0 & \bar{F_{22}} \end{pmatrix}, \quad \Omega_4 = \begin{pmatrix} 0 & -(\bar{F_{21}}\dot{\theta_1} + \bar{F_{22}}\dot{\theta_2}) & 0 \\ (\bar{F_{21}}\dot{\theta_1} + \bar{F_{22}}\dot{\theta_2}) & 0 & -(F_{11}\dot{\theta_1} + F_{12}\dot{\theta_2}) \\ 0 & F_{11}\dot{\theta_1} + F_{12}\dot{\theta_2}) & 0 \end{pmatrix}$$

When these expressions are substitute in equation no. 4.32, we get

$$T_4^T W_4 M_4 T_4 = 0, \quad \Rightarrow T^T W M T = 0 \tag{4.33}$$

So the Convective inertia matrix C of equation 4.9 evaluate to

$$\begin{aligned} C = (m_c r^2/4)\Bigg[& \begin{pmatrix} 6F_{11}\dot{F_{11}} + \bar{F_{21}}\dot{F_{21}} & 6F_{11}\dot{F_{12}} + \bar{F_{21}}\dot{F_{22}} \\ 6\dot{F_{11}}F_{12} + \dot{F_{21}}\bar{F_{22}} & 6F_{12}^2\bar{F_{22}} \end{pmatrix} \\ & + \begin{pmatrix} 6G_{11}\dot{G_{11}} + \bar{G_{21}}\dot{G_{21}} & 6G_{11}\dot{G_{12}} + \bar{G_{21}}\dot{G_{22}} \\ 6\dot{G_{11}}G_{12} + \dot{G_{21}}\bar{G_{22}} & 6G_{12}^2\bar{G_{22}} \end{pmatrix} \Bigg] \end{aligned} \tag{4.34}$$

All the components of the equation 4.9 have now been evaluated, except the τ. These are simply the torque exerted by the actuated wheel. This completes the dynamic model of the WMR with generalized caster wheel configuration.

4.3 Special cases

4.3.1 Standard caster ($d_1 = 0$)

The standard caster wheel configuration can be obtained by setting the value of $d_1 = 0$. In such condition the left hand side matrix of equation 4.19 and 4.20 becomes a diagonal matrix. Therefore, the first and second equation of 4.19 and 4.20 gets divided by d_2 and r respectively. The resulting equations relating the unactuated joint rate to actuated joint rates are similar to those reported by [22],[23].

4.3.2 Under Actuated Case ($d_2 = 0$)

It can be seen from equation 4.19, that when the *caster offset* $d_2 = 0$, the LHS matrix becomes singular. So the unactuated joint rates cannot be determined from $\dot{\theta_a}$. It is therefore essential to have proper caster offset in case we need caster like behaviour from a passive wheel.

Another solution is to put an extra actuator to control the bracket motion by controlling ψ_i. As in the case of ackerman steering mechanism, where the steering wheel controls the orientation of the front passive wheels of a car.

4.4 Simulation of The Mobile Platform

The mobile manipulator was modelled as differential drive robot, the front wheels and steering mechanism was not included in the dynamic model as there mass are too small compared to the mobile platform. The weight of a wheel is 300g, the steering mechanism 240g, where as the weight of platform is 70Kg.

In the simulation the vehicle (point 03), is required to traces a circle of radius 5m and with Îš(t) as given below.

$$\beta(t) = \frac{20\pi}{60^3}t^3 + \frac{30\pi}{60^4}t^4 + \frac{2\pi}{60^5}t^5 \tag{4.35}$$

4.5 Inverse Dynamics

Using the Inverse Kinematic, the wheel velocity and acceleration are determined using pseudo Inverse from the equation given below. Where r is radius of the wheel and θ_i is the wheel roll angle of wheel #1 and #2. The platform angular velocity is ω and the Cartesian velocity of point o3 is given by $\dot{x}, \dot{y}$ in body coordinate system

The wheel angle, velocity and acceleration are used in the dynamic equation to calculate the torque required by each motor. The results are plotted in figure

2. The size of generalized inertia matrix, and convective term are not reported here as there are size is very large.

The equation of dynamic model is given in equation 4.36, where θ_l, θ_r are the rear left and right wheel role angles, $t_i^T = [\omega_i, v]$ the twist, m_i the mass, I_i the inertia of individual bodies.

$$
\begin{aligned}
& T^T M T\ddot{\theta}_a = -T^T(M\dot{T} + WMT)\dot{\theta}_a + T^T(w^J + w^G) \\
& where \quad \theta_a = [\theta_l, \theta_r]^T, \quad [t_1, t_2, t_3] = (T\dot{\theta}_a)^T, \quad M = diag(M_1, M_2, M_3) \\
& \qquad W = diag(W_1, W_2, W_3), \quad W_i = \begin{pmatrix} \omega_i \times 1 & 0 \\ 0 & 0 \end{pmatrix}, \quad M_i = \begin{pmatrix} \omega_i \times I_i & 0 \\ 0 & m_i \end{pmatrix}
\end{aligned} \tag{4.36}
$$

w^G and w^J represents the gravitational force and the external torque/Force applied by motor respectively.

The torque required at wheels for the vehicle to move up a spiral ramp of slope 10^o and radius 5m is given figure 4.4. The numerical values used for the forward dynamic simulation is given in table 4.1.

Table 4.1: Dynamic parameters used in forward dynamic simulation.

Part Name	*Mass Property*	*Value*
Rear Wheels	mass	300g
	Moment of Inertia	diag(242, 242, 465)kg mm^2
Base Frame	mass	70Kg
	Moment Of Inertia	$\begin{pmatrix} 1.18 & 0.01 & -0.05 \\ 0.01 & 1.28 & 0.08 \\ -0.05 & 0.08 & 0.53 \end{pmatrix} Kg - m^2$

4.6 Conclusion

We have presented the dynamic equation of the most general form of caster wheel configuration. Even though we have considered here only two caster wheel the formulation can be extended to any number of caster wheels, in such case we have to find equation 4.19 for each caster wheel system, and then proceed mechanical as to calculate the corresponding twists. We have also shown that the dynamic of

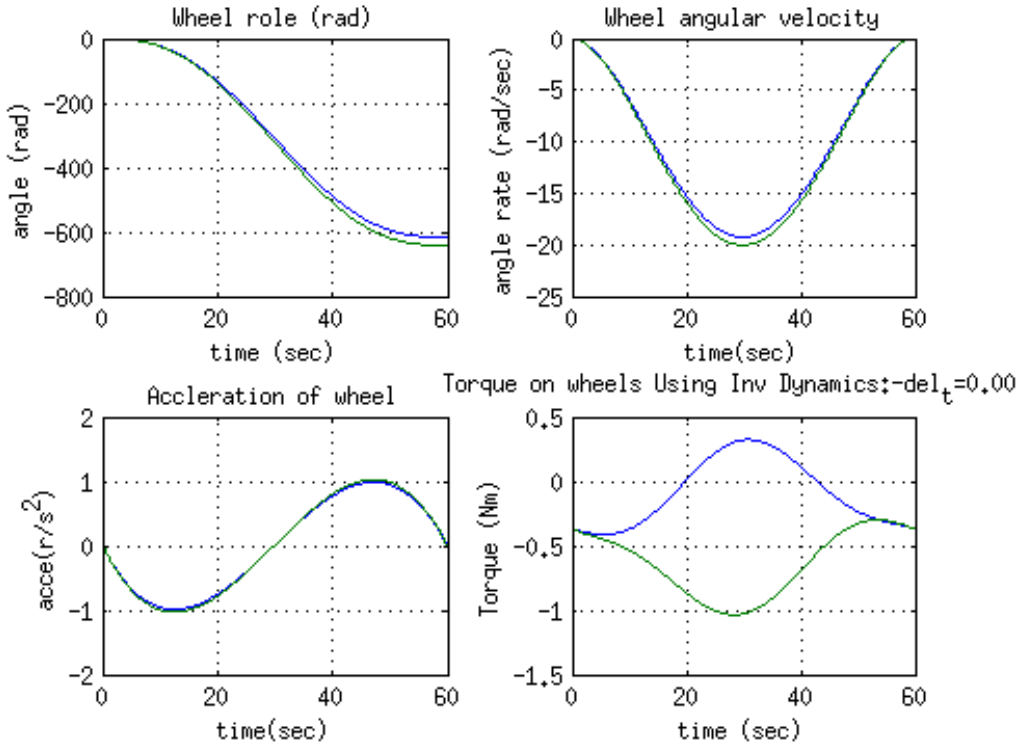

Figure 4.4: Inverse Dynamics of Mobile Robot moving up on 15^o ramp

standard caster wheels is a special case of our general case with $d_1 = 0$. We have also proved why a caster needs a non-zero caster offset distance, and the need of extra actuators in case $d_2 = 0$.

4.7 Summary

In this chapter,

Chapter 5

Control

In this chapter the control architecture of the teleoperated mobile robot is presented. The user interface for teleoperation is discussed. The control algorithm running on the mobile robot and the hardware used for the control of traction and steering is discussed. The protocol used for communication between the robot and user interface also described in detail.

5.1 Control Architecture and Hardware

The mobile manipulator is planned to be teleoperated over a wireless network. The control block diagram and architecture are shown in Figure 5.1. It has a remote control station which is the interface for the operator and a local controller on the

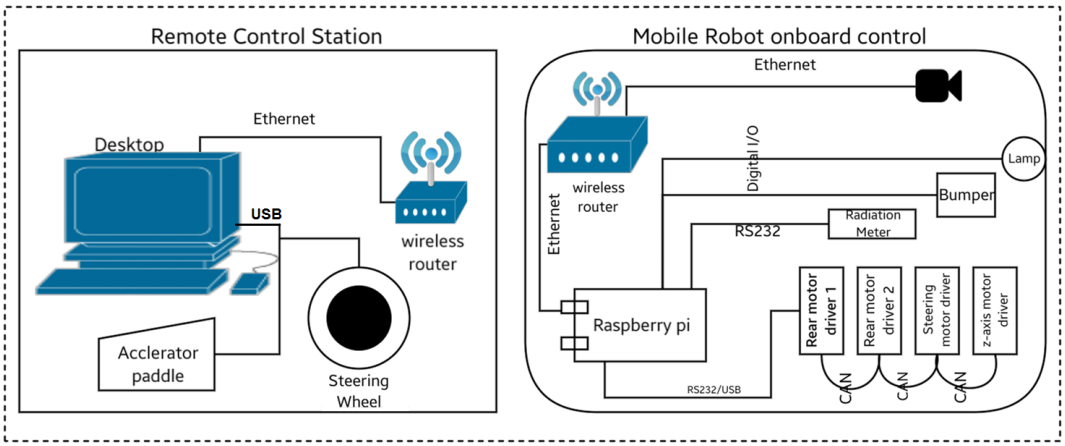

Figure 5.1: Control Architecture Block Diagram

mobile manipulator. They communicate over a wifi network. The remote station send data packet every 50 millisecond to the mobile manipulator. The commanded velocity, the steer angle, the z position of the platform and the state of the detector and headlamps constitutes the data packet sent by the remote station. The on board control of the mobile robot replies with a data packet consisting of the X, Y position and orientation θ of the robot, the current steer angle, angular velocities of each wheels, the z position of the top platform, battery voltage and bumper status.

5.1.1 Local Onboard Controller

The on-board computer which is Raspberry Pi running raspian (linux) os receives the command from the remote station and controls the robot hardware through customized c++ application. The raspberry pi is daisy chained to the four Maxon EPOS2 motor controllers/drivers. The communication between the onboard computer and the first Maxon controllers is over usb/RS232 interface using Maxon's proprietorial protocol [25]. The first controller serves as CAN master for the rest of the controllers. The rear wheel motor drivers are configured in velocity servo loop. The steering and the z-axis motors drivers are configured in position control loop. The camera mounted on the mobile robot and Raspberry Pi is connected over Ethernet via a wireless hub. the wiring digram of the robot is given figure 5.2.

5.1.1.1 The Motor Controller

Describe the velocity loop and position loop. Put figure of responce of each motor for given KP KI KD value

5.1.1.2 The control Algorithm

- steering kinematic equation
- Sequence of program flow

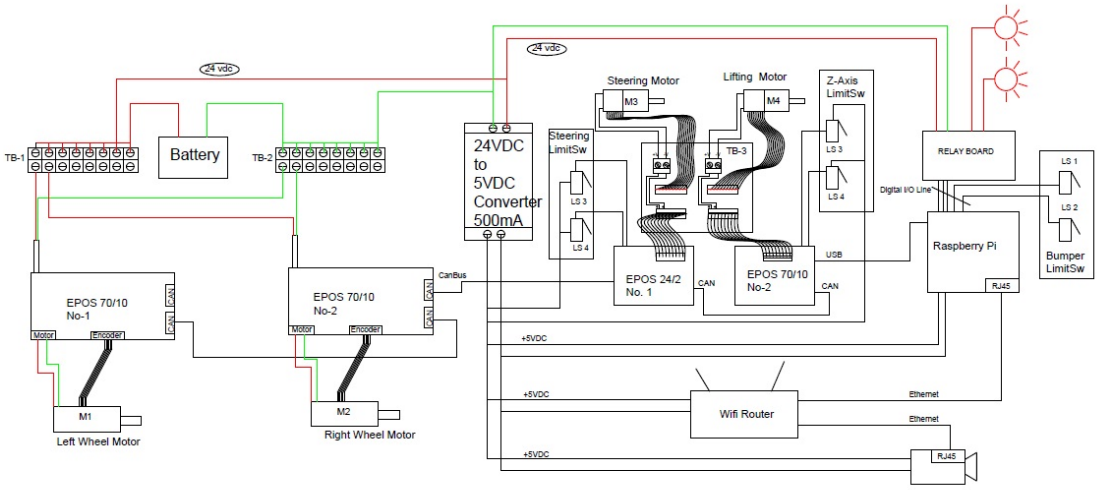

Figure 5.2: Wiring Diagram of Robot

- data structure of command and comand exexution frequency

5.1.1.3 Control of Z platform

5.1.1.4 Odometry

5.1.2 The Remote Control Station

The local station consists of a desktop computer running Windows XP. A Steering wheel and two foot switches are connected to the desktop. The steering wheel is used for turning mobile robot. One of the two foot switch acts as an accelerator to set the mean velocity the other is used to brake the vehicle.

The screen of the desktop displays the video streaming from the mobile robot on board camera. A graphical user interface (GUI) also displays the robot's parameters such as current steer angle, velocity of each rear wheel and the position of the z-axis. Buttons on the GUI operates the z-axis, head lamps, etc.

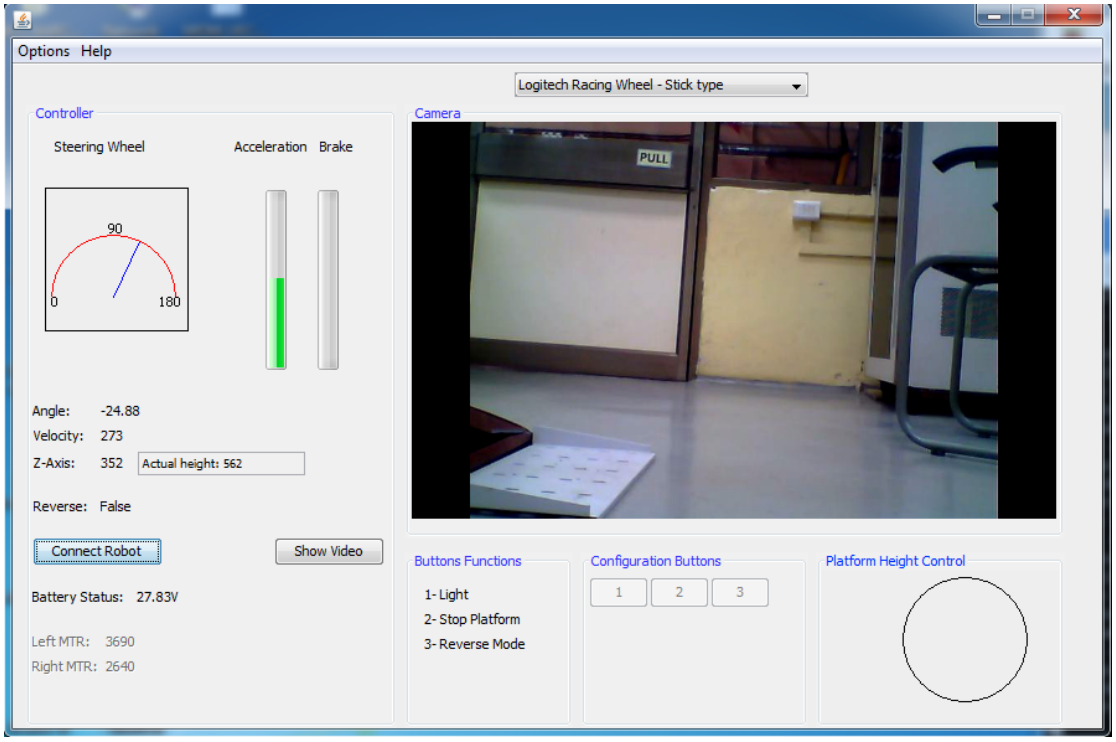

Figure 5.3: User Interface for teleoperation

5.2 Admissible path

5.3 Trajectory Tacking

5.4 Summary

In this chapter,

Chapter 6

Simulation Time Delay Tele-operation

In this chapter simulation of a teleoperated mobile platform is presented. In teleoperation the human operators observe a remote scene through camera/s, and manipulating the local steering wheel and accelerator paddle as shown in figure 6.1 . The command is transmitted to the mobile robot over wireless network. The operator response is based on the latest feedback images from the cameras. In general there is time lag when communication take place over wireless network. The time lag deteriorates the human performance as discussed in [26] and references there in. The this chapter simulation of teleoperation both for delayless and delay transmission network are presented.

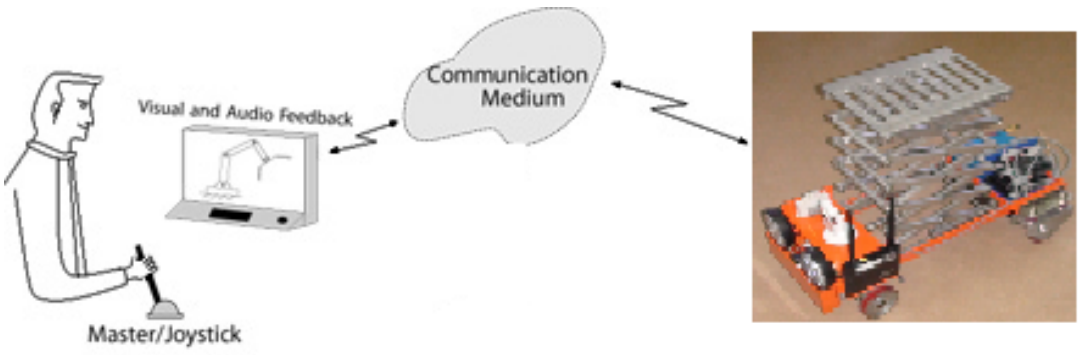

Figure 6.1: Teleoperation Architecture

6.1 Modeling of mobile platform

The standard kinematic model as described in [15] of the mobile platform is used for the simulation. This use of kinematic is justified as the vehicle is expected to move at relatively slow speed and model is simple. Inputs to the model are left and right rear wheel velocities. The front wheels are steered to satisfy the Ackerman condition as presented in **** and are assumed to attain the desired angle instantaneously. Therefore the robot can be treated as differential drive robot. The kinematic model of the platform is presented below

$$\begin{pmatrix} \dot{x} \\ \dot{y} \\ \dot{\theta} \end{pmatrix} = \begin{pmatrix} \cos\theta & 0 \\ \sin\theta & 0 \\ 0 & 1 \end{pmatrix} \begin{pmatrix} r_w/2 & r_w/2 \\ 1/b & -1/b \end{pmatrix} \begin{pmatrix} \dot{\phi_L} \\ \dot{\phi_R} \end{pmatrix} \tag{6.1}$$

Where , b is the distance between the rear wheels, r_w wheel radius. $\dot{\phi_R}$ and $\dot{\phi_L}$ are the left and right wheel rotational velocity.

The operator station sends the command u_1 and u_2 over the wireless network, in general it will be delayed by δ time. These commands are interpreted by the robot controller as the left and right wheel velocities. Therefore by taking the time delay into consideration we can write

$$\begin{pmatrix} \dot{\phi_R}(t) \\ \dot{\phi_L}(t) \end{pmatrix} = \begin{pmatrix} u_r(t-\delta) \\ u_1(t-\delta) \end{pmatrix} \tag{6.2}$$

The control inputs to the mobile robot u_1 and u_2 are generate by the operator based on the visual data available to him. We next present the model of the human operator to be used for simulation the complete loop.

6.2 Modeling the human operator

In order to simulate the teleoperation loop we need a mathematical model of human operator. The mathematical modelling of the operator‘s action is modelled

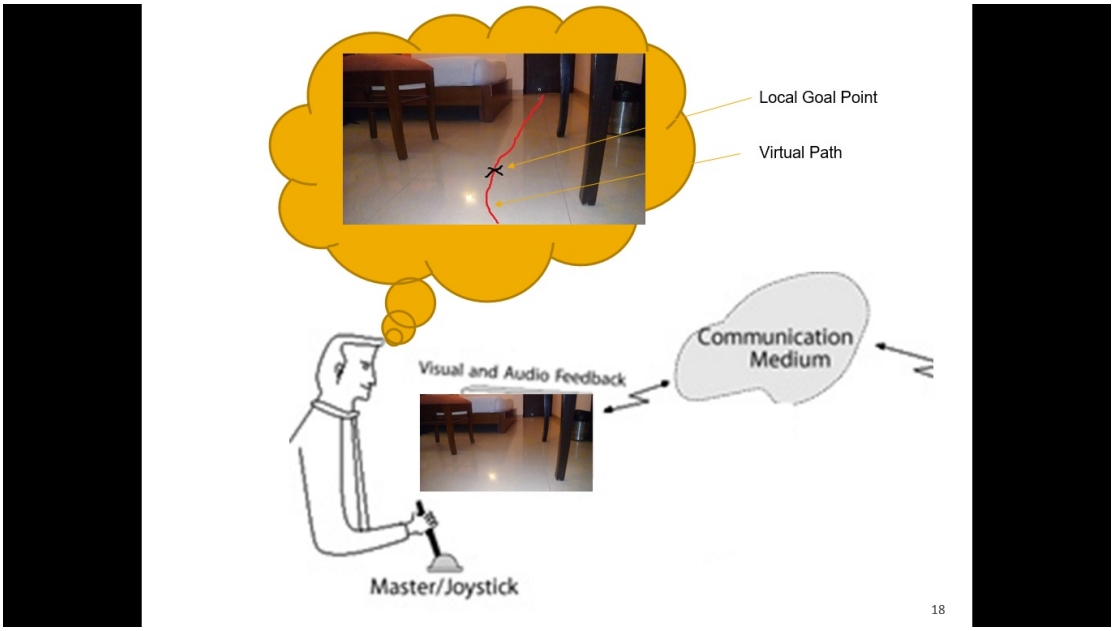

Figure 6.2: Assumed driving strategy

assuming a car driving metaphor. The video feedback, which the he receives of the remote environment, give him the idea of the vehicles position and the tentative next goal point (p) based on a lookahead distance (l). He then constructs a virtual path mentally and tries to manoeuvre or steers the robot to follow that path as shown in figure 6.2. As he moves forward the goal point keeps changing until he reaches the desired location. This methodology of path tracing is known as pure pursuit [27] or following the carrot strategy.

The mathematical model for the pure pursuit method of path following can be derived as given in figure 6.3. As shown in figure 6.3, the origin of the coordinate system is at point o, the middle of rear axis of the robot. Since the differential drive robot can move only about a circle with center lying on the line along its rear axis, a arc op of radius r, is drawn with center $o1$ and passing through o and p. Where p is a point on the path to be traced by the robot. The linear distance l between the points o and p is called the look ahead distance. This distance in the case of a teleoperated robot will depend on the field of view of the remote location camera and the obstacles in present in the remote environment.

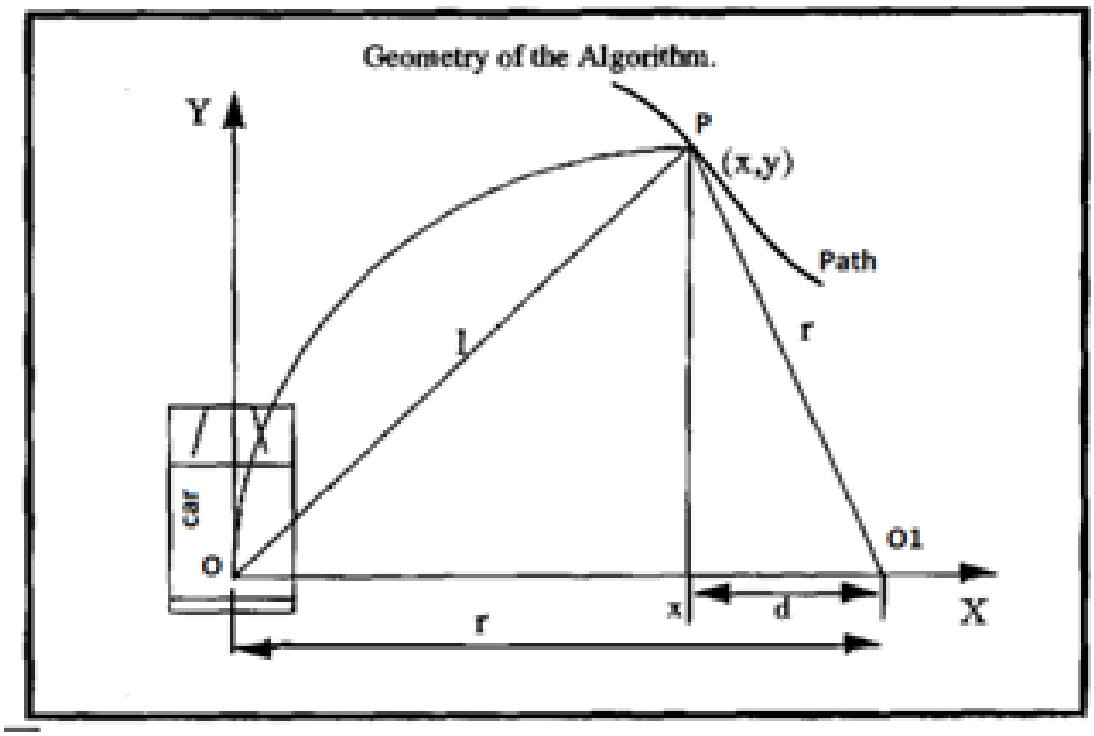

Figure 6.3: Geometry of Pure Pursuit

If (x, y) is the coordinate of point p in $X - Y$ coordinate system, then

$$x^2 + y^2 = l^2, \qquad d = r - x \tag{6.3}$$

Similarly, from triangle $p, x, o1$ we get

$$d^2 + y^2 = r^2 \quad \Rightarrow (r - x)^2 + y^2 = r^2 \quad \Rightarrow x^2 + y^2 - 2rx = 0 \tag{6.4}$$

Replacing x^2 and y^2 in equation 6.4 with 6.3 we get

$$2rx = l^2 \qquad \Rightarrow r = \frac{l^2}{2x} \tag{6.5}$$

Once, the radius r the desired linear velocity v of robot is known the angular velocity of the vehicle is $\dot{\theta} = -v/r$. The rear wheel desired velocities $\dot{\phi_d}(t)$ and $\dot{\phi_(}t)$ can be calculated from equation 6.1. Where $\dot{y} = v$ and to match the orientation of vehicle with that in figure 6.3 we set $\theta = 90^o$. We get

$$\begin{pmatrix} \dot{x} \\ \dot{y} \\ \dot{\theta} \end{pmatrix} = \begin{pmatrix} 0 & 0 \\ r_w/2 & r_w/2 \\ b/2 & -b/2 \end{pmatrix} \begin{pmatrix} \dot{\phi_L} \\ \dot{\phi_R} \end{pmatrix} \quad \Rightarrow \begin{pmatrix} \dot{\phi_L} \\ \dot{\phi_R} \end{pmatrix} = \begin{pmatrix} 1/r_w/ & 1/r_w \\ 1/b & -1/b \end{pmatrix} \begin{pmatrix} v \\ \dot{\theta} \end{pmatrix} \tag{6.6}$$

The operator station sends v and $\dot{\theta}$ as the command over the communication network to the robot. Therefore

$$\begin{pmatrix} u_r(t) \\ u_1(t) \end{pmatrix} = \begin{pmatrix} 1/r_w/ & 1/r_w \\ 1/b & -1/b \end{pmatrix} \begin{pmatrix} v \\ \dot{\theta} \end{pmatrix} \tag{6.7}$$

6.3 Simulation and Results

The teleoperation loop consists the operator model described in section 6.2 at one end of the communication link and Mobile robot model described in 6.1 on the other link. As shown in figure 6.4there will a delay in both direction of communication. In real system the video image is streamed by the robot. Due to large quantity of data and limited bandwidth the delay $h_1 >> h_2$. The amount of delay h_1 was measured and it was found around 0.5sec as described in appendix A. The command sent by the operator is v and $\dot{\theta}$ which is few bites only. Therefore in simulation $h_2 = 0$ is assumed.

6.3.1 The Simulation Algorithm

- Convert the path from global coordinate system (CS) to Robot Local CS
- With a given look ahead distance (l) search for a point on the path
  - If point is found goto step 3
  - If not found increase look ahead distance
- Determine the turning radius (r) using eqnation 6.5

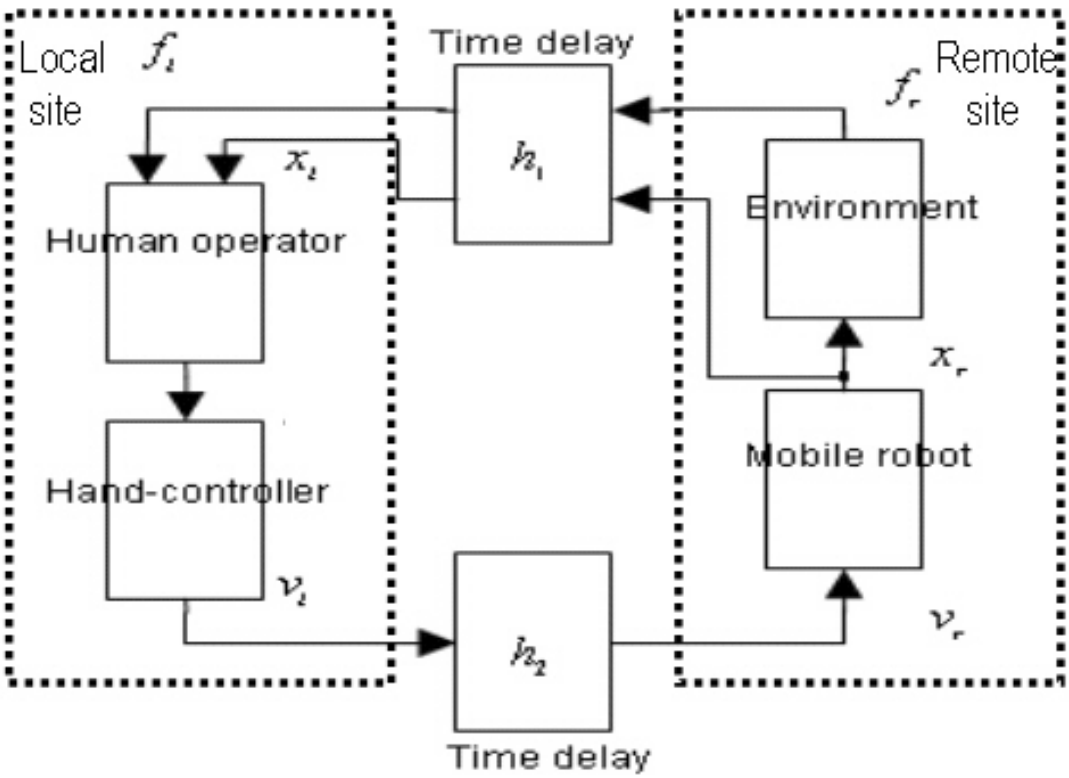

Figure 6.4: Teleoperation block diagram

- Calculate the command to the robot from equation 6.7. Note that these commands are based on the old visual data the operator see.
- Solve delayed differential equation in Matlab using *dde24*.

Simulation was carried using Matlab. Delay differential equation solver dde24 was used to solve equation 6.1 and 6.2 with delayed inputs u_r and u_l. The path tracked was a circle of radius 5m centred at origin of the global coordinate system. The human action was modelled with look ahead distance of 0.5m and linear velocity of 0.5m/s. The initial position of the robot was (4.5,0.0).

The performance of the system with zero delay, i.e. $h_1 = h_2 = 0$ is shown in figure 6.5. Figure 6.6 and 6.7 shows the plot robot motion under delay of 0.5 and 0.8 sec. It is seen that oscillation becomes visible at 0.5sec delay and with 0.8 sec delay the system is on the verge of instability.

It was also observed that the with large vehicle velocity, v and large look ahead distance, l the instability commences with smaller time delay, δ in equation 6.2.

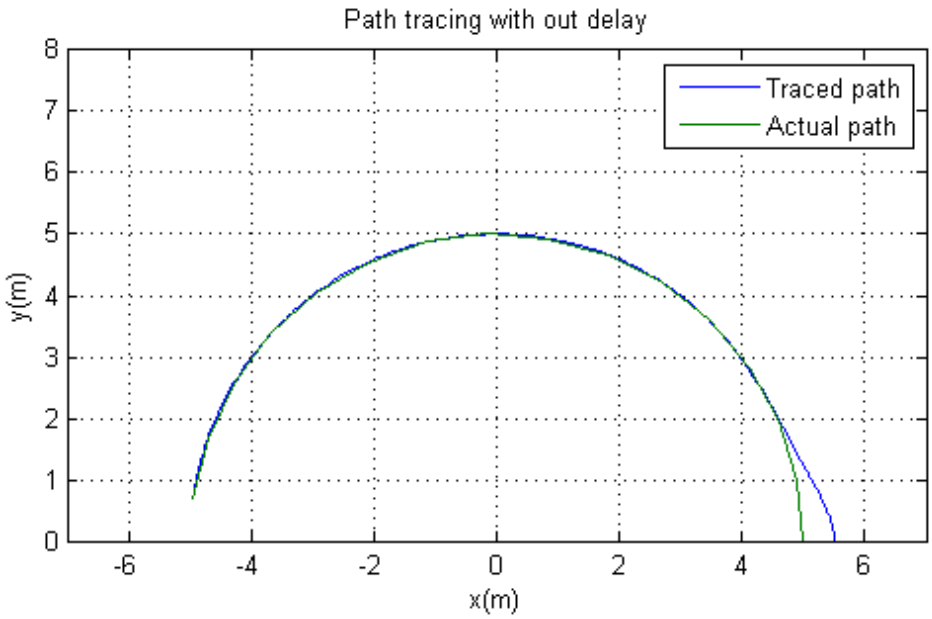

Figure 6.5: Simulation with no time delay in either direction

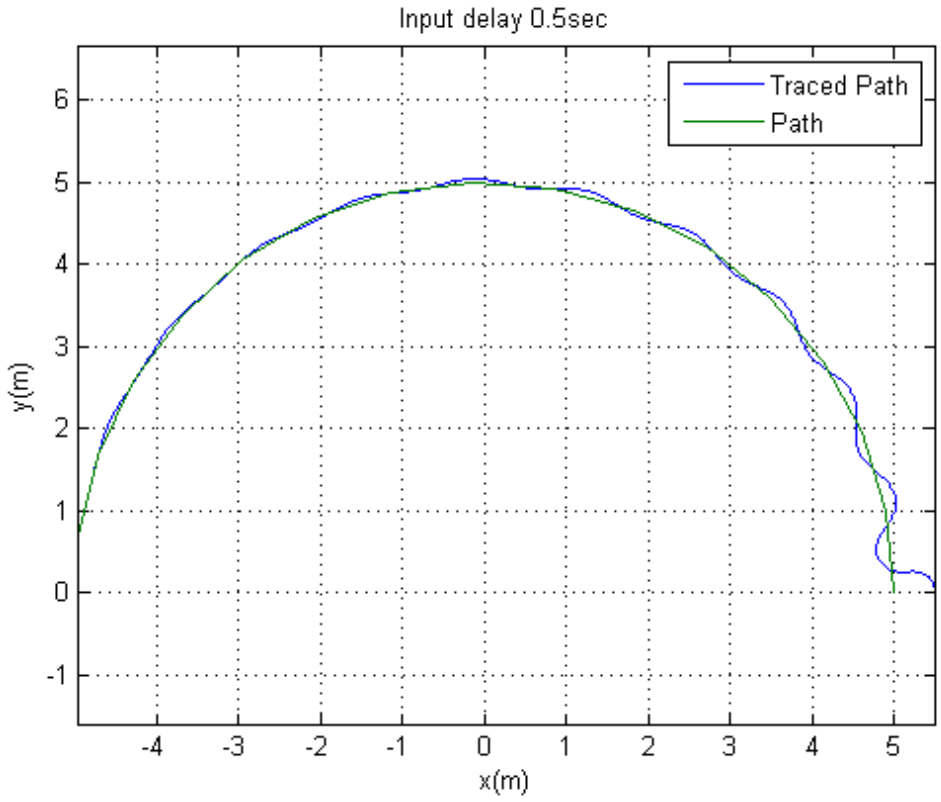

Figure 6.6: Simulation with time delay $h_1 = .5sec$ and $h_2 = 0$

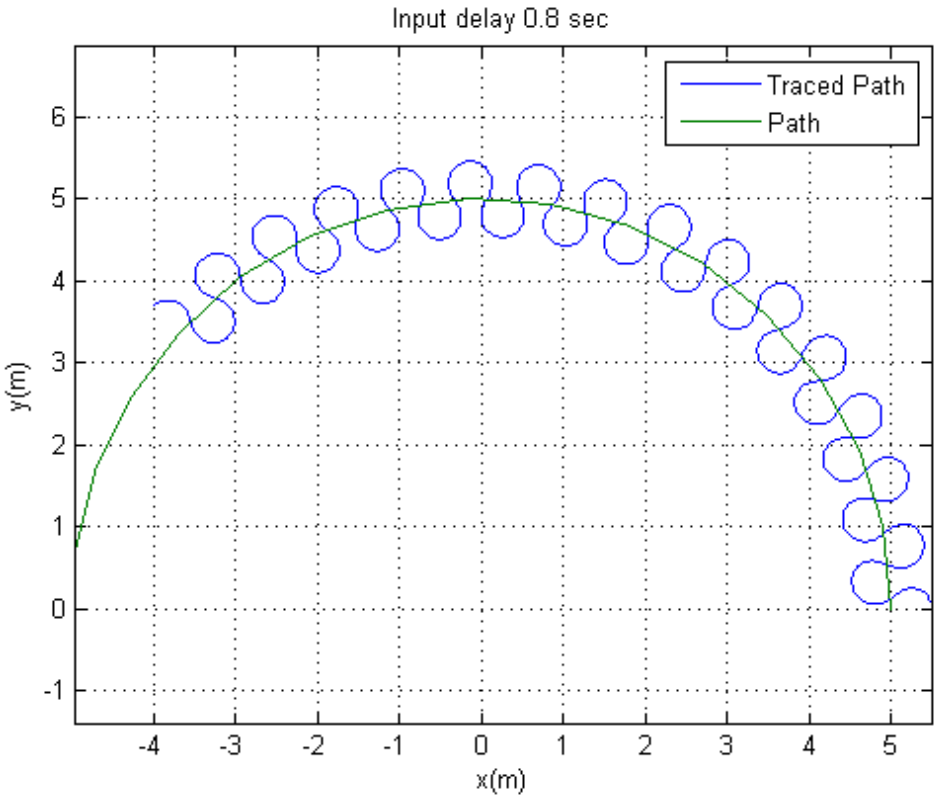

Figure 6.7: Simulation with time delay $h_1 = .8sec$ and $h_2 = 0$

6.4 Summary

In this chapter, simulation study of a teleoperated mobile robot was presented. A mathematical model was presented of the human operator action while driving the robot base on visual feed back. It was shown in by the simulation results that the behaviour of the system deteriorates with increase in delay in communication between the local and remote station. With large time delay the system becomes unstable.

In the next section we propose a predictive model based feedback control which is used to stabilize robot motion under time delay teleopration.

Chapter 7

Predictive Display

In the last chapter it was shown using simulation results that time delay between the remote and local station leads the system towards in stability. In this chapter we use predictive display to alleviate the above problem.

Predictive display has been defined as using the computer for extrapolating the display forward in time [28]. In this a local model of the remote scene is used to predict and render the remote scene in response to operator command. It replaces the delayed video feedback with extrapolated synthesised image of the remote environment and local enables the operator to perform the task normally.

7.1 Remote Scene Extrapolation

The visual data present in the current frame is the view that the robot has seen h_1 second earlier. In order to predict the current scene that the robot might be seeing we need to estimate the current position of the robot. Once the current position of the robot is known we re-construct a view form the old scene by moving the view point to the current position of the robot. To explain this further and to use it in the teleoperation simulation model discussed in chapter 6

7.1.1 here

Chapter 8

Conclusions

This chapter includes the thesis summary, major contributions and future scope of the work.

8.1 Thesis Summary

8.2 Future Scope of the work

The thesis opens up the following future directions:

(i) The

(ii) The

(iii) The

(iv) Implementing

Bibliography

[1] Y. Yamamoto and X. Yun, "Coordinating locomotion and manipulation of a mobile manipulator," in *Decision and Control, 1992., Proceedings of the 31st IEEE Conference on*, pp. 2643–2648, IEEE, 1992.

[2] S. Rajendran and et.al., "Mobile robot for reactor vessel inspection," in *National Conference on Advanced Manufacturing and Robotics*, pp. 2527–2532, CMERI, Durgapur,WB,, 2004.

[3] S. K. Saha and J. Angeles, "Kinematics and dynamics of a three-wheeled 2-dof agv," in *Robotics and Automation, 1989. Proceedings., 1989 IEEE International Conference on*, pp. 1572–1577, IEEE, 1989.

[4] F. G. Pin and S. M. Killough, "A new family of omnidirectional and holonomic wheeled platforms for mobile robots," *IEEE transactions on robotics and automation*, vol. 10, no. 4, pp. 480–489, 1994.

[5] J. E. M. Salih, M. Rizon, S. Yaacob, A. H. Adom, and M. R. Mamat, "Designing omni-directional mobile robot with mecanum wheel," *American Journal of Applied Sciences*, vol. 3, no. 5, pp. 1831–1835, 2006.

[6] J. Suthakorn, S. S. H. Shah, S. Jantarajit, W. Onprasert, W. Saensupo, S. Saeung, S. Nakdhamabhorn, V. Sa-Ing, and S. Reaungamornrat, "On the design and development of a rough terrain robot for rescue missions," in *Robotics and Biomimetics, 2008. ROBIO 2008. IEEE International Conference on*, pp. 1830–1835, IEEE, 2009.

[7] M. Guarnieri, R. Debenest, T. Inoh, E. Fukushima, and S. Hirose, "Development of helios vii: an arm-equipped tracked vehicle for search and rescue operations," in *Intelligent Robots and Systems, 2004.(IROS 2004). Proceedings. 2004 IEEE/RSJ International Conference on*, vol. 1, pp. 39–45, IEEE, 2004.

[8] K. Nagatani, S. Tachibana, M. Sofne, and Y. Tanaka, "Improvement of odometry for omnidirectional vehicle using optical flow information," in *Intelligent Robots and Systems, 2000.(IROS 2000). Proceedings. 2000 IEEE/RSJ International Conference on*, vol. 1, pp. 468–473, IEEE, 2000.

[9] J. Y. Wong, *Theory of ground vehicles*. John Wiley & Sons, 2008.

[10] T. Bevan, *Theory of Machines, Third Edition*. Delhi, India: CBS Publishers & Distributors, 1984.

[11] *Motor catalogue 2014.* Switzerland: Maxon Motors, 2017.

[12] J. T. Machado and M. F. Silva, "An overview of legged robots," in *International symposium on mathematical methods in engineering*, MME Press Ankara, Turkey, 2006.

[13] K. P. Valavanis and G. J. Vachtsevanos, *Handbook of unmanned aerial vehicles.* Springer Publishing Company, Incorporated, 2014.

[14] J.-B. Mouret, *Evolutionary Adaptation in Natural and Artificial Systems.* PhD thesis, Université Pierre et Marie Curie, 2015.

[15] G. Campion, G. Bastin, and B. Dandrea-Novel, "Structural properties and classification of kinematic and dynamic models of wheeled mobile robots," *IEEE transactions on robotics and automation*, vol. 12, no. 1, pp. 47–62, 1996.

[16] G. Campion and W. Chung, "Wheeled robots," in *Springer Handbook of Robotics*, pp. 391–410, Springer, 2008.

[17] R. M. DeSantis, "Modeling and path-tracking control of a mobile wheeled robot with a differential drive," *Robotica*, vol. 13, no. 04, pp. 401–410, 1995.

[18] K. C. Koh and H. S. Cho, "A smooth path tracking algorithm for wheeled mobile robots with dynamic constraints," *Journal of intelligent & robotic systems*, vol. 24, no. 4, pp. 367–385, 1999.

[19] B. d'Andréa Novel, G. Campion, and G. Bastin, "Control of nonholonomic wheeled mobile robots by state feedback linearization," *The International journal of robotics research*, vol. 14, no. 6, pp. 543–559, 1995.

[20] B. d'Andrea Novel, G. Bastin, and G. Campion, "Modelling and control of non-holonomic wheeled mobile robots," in *Robotics and Automation, 1991. Proceedings., 1991 IEEE International Conference on*, pp. 1130–1135, IEEE, 1991.

[21] K. Thanjavur and R. Rajagopalan, "Ease of dynamic modelling of wheeled mobile robots (wmrs) using kane's approach," in *Robotics and Automation, 1997. Proceedings., 1997 IEEE International Conference on*, vol. 4, pp. 2926–2931, IEEE, 1997.

[22] S. K. Saha and J. Angeles, "Dynamics of nonholonomic mechanical systems using a natural orthogonal complement," *Journal of Applied Mechanics*, vol. 58, no. 1, pp. 238–243, 1991.

[23] J. Angeles, *Fundamentals of robotic mechanical systems: theory, methods, and algorithms*, vol. 124. Springer Science & Business Media, 2013.

[24] S. Saha, *Introduction to robotics.* Tata McGraw-Hill, New Delhi, 2010.

[25] *EPOS Application Note: RS232 to CANopen Getway.* Maxon Motors, 2012.

[26] J. Y. Chen, E. C. Haas, and M. J. Barnes, "Human performance issues and user interface design for teleoperated robots," *IEEE Transactions on Systems, Man, and Cybernetics, Part C (Applications and Reviews)*, vol. 37, no. 6, pp. 1231–1245, 2007.

[27] R. C. Coulter, "Implementation of the pure pursuit path tracking algorithm," tech. rep., Carnegie-Mellon UNIV Pittsburgh PA Robotics INST, 1992.

[28] S. T. B, "Space teleoperation through time delay: review and prognosis," *IEEE Transactions on Robotics and Automation*, vol. 9, no. 5, October 1993.

Appendix A

Simulation Time Delay Tele-operation

A.1 Measurment of Time Delay in Video Feedback

The experimental method used to find the delay in video stream coming from the remote station is described here.

Appendix B

Dynamics

B.1 Inertia Dyad

The dyadic product takes two vector and returns a second-order tensor. If $\mathbf{a}$ and $\mathbf{b}$ are two vectors expressed as $\mathbf{a} \equiv a_1\mathbf{i} + a_2\mathbf{j} + a_3\mathbf{k}$ and $\mathbf{b} \equiv b_1\mathbf{i} + b_2\mathbf{j} + b_3\mathbf{k}$. Then the dyadic product of $\mathbf{a}$ and $\mathbf{b}$ are defined as:

Publications from the Thesis

Research papers published/presented/under preparation are listed below

1. Hayat, A.A., Abhishek, V., Saha, S.K., Dynamic Identification of Manipulator: Comparison between CAD and Actual Parameters, 17*th National and 2nd International Conference on Machine and Mechanisms, iNaCoMM 2015*, IIT Kanpur, Dec. 16–19, 2015.
2. Udai, A. D., Hayat, A. A., Saha, S. K., "Parallel Active/Passive Force Control of Industrial Robots with Joint Compliance," *IEEE/RSJ International Conference on Intelligent Robots and Systems (IROS 2014), Chicago, Illinois*, Sept. 14–18 , 2014.

Brief Bio-data of the Author